Sixth International Symposium on Marine Propulsors
smp'19, Rome, Italy, May 2019

# Prediction of Unsteady Developed Tip Vortex Cavitation and its Effect on the Induced Hull Pressures *

**Seungnam Kim and Spyros A. Kinnas**

Ocean Engineering Group, Department of Civil, Architecture and Environmental Engineering,
The University of Texas at Austin, Austin, Texas, U.S.

## ABSTRACT

Reducing on board noise and fluctuating pressures on ship surface have been challenging and added value research in the maritime industry. Among the constituent causes for the unpalatable vibrations, propeller-induced pressure has been considered one of the main factors. A numerical method, HULLFPP solves an acoustic Boundary Element Method (BEM) for the diffraction potential on the ship surface and is coupled with a low-order panel method, PROPCAV [9] to account for the effects of propeller, trailing wake, and the sheet cavity on propeller surface.

This paper is a continuation of the work presented in SMP'17 [14] in which a sequence of numerical methods is applied to effectively predict the propeller-induced hull pressures given the hull/rudder/propeller geometries in fully-wetted case. The importance of the unsteady wake alignment model in periodic non-axisymmetric inflow was addressed in SMP'17. In this paper, HULLFPP is extedned to cavitating propellers including the developed tip vortex model, which was initially proposed by Lee 2004 [11].

To this end, a hybrid BEM/RANS method, PC2NS [16] is first used to evaluate the effective wake at propeller plane. Then, PROPCAV is used to evaluate the dipole and the source singularities on propeller boundary with consideration of the developed tip vortex. Finally, HULLFPP is used to calculate the fluctuating hull pressures by solving the acoustic BEM. Results are compared to the published experimental data, and the influence of different tip vortex radii on ship hull pressure is investigated.

## KEYWORDS

Hull pressure, Boundary element method, Developed tip vortex, Unsteady wake alignment model, Diffraction potential.

## 1 INTRODUCTION

From the time people started to use propellers as a prime propulsion system for maneuvering ships, reducing propeller-induced noise and fluctuating pressures over ship surface have been one of the most challenging and added value research topics. Among the constituent causes for the noise and vibrations, propeller-induced hull pressure has been attributed as one of the main factors, and many efforts have been given to predict and reduce it through numerical and experimental approaches [3, 4, 6].

First, experiments have been conducted to predict both the noise level and hull pressure signals by Hallander & Lars 2013 [4]. They performed the experiments with a model-scaled ship with eight pressure transducers mounted on the hull surface above the propeller in order to record the propeller-induced hull pressures. On the other hand, as a numerical approach, BEM has been a proper tool to predict the propeller-induced hull pressure since it significantly reduces computing time compared to other commercial RANS solvers. Most of the BEM applications focus on the effect of cavitation on hull pressure since the cavitation is the main contributor of high-level noise and vibrations (Seol et al. 2005 [13] & Lee et al. 2014 [12]). For a cavitating propeller, the cavitation source is the major excitation in the acoustic BEM model so that the influence of the propeller lifting force, blade thickness, and the blade trailing wake can be neglected.

In the previous works presented in SMP'17 [14] and CAV'18 [10], fluctuating hull pressure is measured numerically using HULLFPP in wetted and cavitating conditions, respectively, but the effects of the developed tip vortex were not included. Even though omitting inception stage of tip vortex cavity is far from its physical development, observed in the experiment (Hallander & Lars 2013 [4]), predicted pressure signals qualitatively corresponded to the experimental measurements at most transducers. Due to the discrete singularity arrangement used to represent the tip vortex at the wake tip, hull pressure is very sensitive to the distance from the tip vortex. In the inclined inflow, for example, tip vortex has significant effects on hull pressure downstream and is expected to affect less when passing under propeller shaft due to the relatively large distance from the control points on the hull.

In order to investigate the effect of the developed tip vortex on the unsteady hull pressure, a series of numerical methods is applied in sequence as follows:

- First, BEM/RANS interactive scheme (PC2NS) is used to evaluate the effective wake on propeller plane.
- PROPCAV employs the unsteady wake alignment scheme to allow the physical variation of trailing wake with blade angle under the predicted periodic

*Corresponding Author, Seungnam Kim: naoestar@utexas.edu

non-axisymmetric inflow.

- Then, the developed tip vortex model, which was initially proposed by Lee 2004 [11], is mounted on the aligned trailing wake behind the blade trailing edge.
- The unsteady cavity problem, including the sheet cavity on the blade and the developed tip vortex, is solved for the singularities (discrete vortex and source strength) over the propeller and sheet/tip vortex cavity boundaries.
- The induced potentials on the ship hull due to a propeller, its wake, sheet cavity, and the developed tip vortex cavity are determined by solving Green's formula in HULLFPP.
- Finally, a pressure-BEM solver is used to predict the diffraction pressure which leads to the solid boundary factor to estimate the fluctuating hull pressure.

As a preliminary study of the effect of the developed tip vortex on the hull pressure, tip vortex radius is assumed to be constant and does not change with blade angle in this work. In order to validate the results from the present method, The predicted hull pressure signals are compared to the experimental data. Besides, Full-blown RANS simulations are also conducted to compare the contour plots of vorticity in wake from RANS with the trailing wake predicted by BEM using the unsteady wake alignment scheme.

## 2 METHODOLOGY

### 2.1 The Unsteady Wake Alignment Scheme

The unsteady wake alignment model was first introduced by Lee 2004 [11] and has been recently improved by Kim 2017 [7]. Su et al. 2018 [15] first employed the unsteady alignment model in calculating the hull pressure, and it is shown that the unsteady wake behaves better in terms of predicting the downstream hull pressures in fully-wetted case. One of the major improvements is to couple the unsteady alignment algorithm with the Full Wake Alignment (FWA) scheme (Tian and Kinnas 2012 [17] & Kim et al. 2018 [8]), which models the trailing vortices as material lines, following the local stream in steady state. As results, both the numerical stability and the correlations with RANS results have been improved. In addition, various input conditions, i.e., effective wake and propeller geometry can be considered in unsteady calculations.

The basic algorithm for unsteady wake alignment is similar to the steady case, but the time variation of incoming flow needs to be included in evaluating the total velocity in the flow field where wake panels are placed after the alignments. The alignment starts with the FWA in steady state using only the zeroth harmonic ($t = 0$) in the effective wake, and proceeds into the unsteady alignment procedure ($t > 0$) using the Euler-explicit scheme with full harmonics in a progressive manner, as shown in Equation (1). It normally takes 3 to 5 revolutions for a wetted case to achieve the converged force predictions (thrust and torque coefficients) in the hydrodynamic BEM. A detailed description of the unsteady wake alignment model coupled with the FWA can be found in Kim 2017 [7].

$$\begin{aligned} X_{i+1}^{n+1} &= X_i^n + \frac{1}{2}(\vec{U}_{T_{X_i}}^n + \vec{U}_{T_{X_{i+1}}}^n)\Delta t \\ Y_{i+1}^{n+1} &= Y_i^n + \frac{1}{2}(\vec{U}_{T_{Y_i}}^n + \vec{U}_{T_{Y_{i+1}}}^n)\Delta t \\ Z_{i+1}^{n+1} &= Z_i^n + \frac{1}{2}(\vec{U}_{T_{Z_i}}^n + \vec{U}_{T_{Z_{i+1}}}^n)\Delta t \end{aligned} \quad (1)$$

where $i$ and $n$ denote the $i$th node point at the $n$th time step, $\vec{U}_T$ is the total velocity, and $\Delta t$ is the time step size. $X, Y$, and $Z$ are the coordinates of the nodal points on the wake surfaces.

### 2.2 Modeling Developed Tip Vortex

The flow around the blade tip, from the pressure side to the suction side, produces the tip vortex, which flows from the blade tip to downstream. The tip vortex cavity usually starts downstream of the propeller tip in a detached form, and as the cavitation number decreases, the detached tip vortex cavity moves closer to the blade tip (developed tip vortex). In this paper, tip vortex cavity is assumed to be always attached to the blade tip throughout the propeller revolutions at the given cavity number. Also, the tip vortex radius is constant to have the uniform circular section over its axial length, which is the same as the wake length. In practice, these assumptions are generally invalid since the tip vortex starts to develop from somewhat downstream, as shown in Figure 9, and the tip vortex radius should be changing depending on the downstream locations in order to satisfy the dynamic boundary condition on its surface. Even though the above assumptions deviate from the physical inception of the tip vortex, the aim of this paper is to focus on the effect of changing tip vortex radius on the propeller-induced hull pressure as a preliminary study.

The solution in the BEM solver is determined in the propeller fixed coordinates. The total inflow velocity relative to the propeller is defined as follows:

$$\vec{U}_{in}(x,y,z,t) = \vec{U}_w(x, r, \theta - \omega t) + \vec{\omega} \times \vec{x}(x,y,z) \quad (2)$$

where $r = \sqrt{y^2 + z^2}$, $\vec{x} = (x, y, z)$, and $\theta = \tan^{-1} z/y$. Since the fluid is assumed to be inviscid, and the flow to be irrotational and incompressible, the fluid domain can be represented by using the perturbation potential, $\phi(x, y, z, t)$, which is time dependent as follows:

$$\vec{q}(x,y,z,t) = \vec{U}_{in}(x,y,z,t) + \nabla\phi(x,y,z,t) \quad (3)$$

where $\vec{q}(x, y, z, t)$ is the time dependent total flow velocity. The perturbation potential $\phi(x, y, z, t)$ defined in Equation (3) has to satisfy Laplace's equation, $\nabla^2\phi = 0$; therefore, the potential $\phi$ at any arbitrary point $p$ on both the wetted and cavity surfaces satisfy the Green's third identity as follows:

$$2\pi\phi_p(\vec{x},t) = \iint_{S_{WS}(t)\cup S_T(t)\cup S_C(t)} \left[\phi_q(\vec{x},t)\frac{\partial G(p;q)}{\partial n_q(t)} - \frac{\partial \phi_q(\vec{x},t)}{\partial n_q(t)}G(p;q)\right]dS + \iint_{S_w} \Delta\phi_w(r_q,\theta_q,t)\frac{\partial G(p;q)}{\partial n_q(t)}dS \tag{4}$$

where $G(p;q) = 1/R(p;q)$ is the Green's function, and $R(p;q)$ is the distance between the field point $p$ and the variable point $q$. $\vec{n}_q(t)$ is the unit normal vector to the surfaces of the propeller, its wake, hub, sheet cavity, and developed tip vortex. It points into the fluid domain. $\Delta\phi_w$ is the potential jump across the wake surface $S_w$. $S_{WS}$ represents fully wetted blade and hub surface. $S_T$ and $S_C$ denote the tip vortex cavity and blade sheet cavity surface, respectively. The Green's formula in Equation (4) states that the potentials on the fluid domain can be represented by dipole and source distribution. The unique solution of Equation (4) can be determined by enforcing the boundary conditions on the exact body and cavity surface.

The trajectory of a tip vortex in non-cavitating conditions was found to be close to that of cavitating conditions by Arndt et al. 1991 [1]. Thus, the unsteady wake from fully-wetted runs can be used to predict the trajectory of the developed tip vortex. In this paper, wake geometry is first generated via the unsteady wake alignment scheme, then the initial shape of the tip vortex is assumed to be a solid cylinder with discretized circular cross sections. The cylindrical tip vortex is placed at the wake tip behind the blade trailing edge and follows the trajectory the aligned wake. Given the shape of the tip vortex is initially known, potentials on the tip vortex surface are solved for, together with the potentials on the blade and the hub.

### 2.3 Boundary Element Method: Solver for the Oscillating Hull Pressure

According to the Bernoulli equation, the small amplitude pressure oscillation $P^{(t)}$ can be represented by the steady velocity potential $\Phi^{(t)}$, as shown in Equation (5). In this equation, $\omega$ is the angular velocity of the propeller, $Z$ is the number of blades, and $\Phi_n$ is the velocity potential magnitude at a certain frequency.

$$P^{(t)} = -\rho\frac{\partial\Phi^{(t)}}{\partial t} = -\rho\sum_{n=1,2,\ldots} nZ\omega\Phi_n i e^{inZ\omega t} \tag{5}$$

Instead of solving for the oscillating pressure field, the velocity potential field $\Phi_n$ is solved at different frequencies. The potential field $\Phi_n$ is governed by the Helmholtz equation. For the near-field small-amplitude pressure fluctuation caused by marine propellers, an infinite sound speed can be assumed so that the Helmholtz equation is reduced to a Laplace equation, as shown in Equation (6).

$$\nabla^2\Phi_n = 0 \tag{6}$$

Similar to the hydrodynamic BEM, the $n$th total velocity potential field $\Phi_n$ can be decomposed into a radiated potential field $\Phi_n^{(R)}$ (taken equal to the potential due to the propeller flow in the absence of the hull) and a diffraction potential field $\Phi_n^{(D)}$. The radiated potential field $\Phi_n^{(R)}$ is the Fourier series of the unsteady perturbation potential field in the hydrodynamic BEM, which represent the propeller, hub, and developed tip vortex. The lowest frequency for the Fourier decomposition is the blade-passing frequency $Z(\omega/2\pi)$.

Based on the BEM, the total potential field $\Phi_n$ can be solved by Equation (7) where $S_H$ is the hull surface and $S_I$ is the image of the hull. The unsteady pressure field on the ship hull can be calculated by Equation (7).

$$\frac{1}{2}\Phi_n = \Phi_n^{(R)} - \frac{1}{4\pi}\iint_{S_H+S_I}\Phi_n\frac{\partial G}{\partial n}dS \tag{7}$$

Different from the hydrodynamic BEM model, the total potential, instead of the diffraction potential, is solved. This eliminates the source-induced potentials in the boundary integral equation which saves computation time. However, the method cannot be used for the hydrodynamic BEM model because the total velocity field can be vortical and not governed by the Laplace equation. Constant strength dipole panels are placed on the ship hull surface. The effect from the top tunnel wall is included by the image model. The model-scaled ship contains the rudder, as shown in Figure 4, but the present numerical method does not include the rudder geometry in order to avoid the singular behavior coming from the proximity between the wake panels and the rudder surface. The details about the interaction between wake panels and rudder can be found in He 2017 [5].

## 3 NUMERICAL AND EXPERIMENTAL RESULTS

### 3.1 Unsteady Wake Alignment in $10^\circ$ Inclined Shaft Flow

In order to validate the results from the hydrodynamic BEM using unsteady wake in periodic non-axisymmetric inflow, DTMB 4661 propeller [2] is first tested in $10^\circ$ inclined shaft flow, before including the tip vortex model. DTMB 4661 propeller is a five bladed propeller with a high skew distribution. Hub geometry has an elliptic shape that closes both upstream and downstream. The design advance ratio of this propeller is $J_S = 1.14$. As shown in Figure 1, the direction of the aligned wake is inclined toward the free surface since the incoming flow has relatively faster axial velocity around the ship bottom.

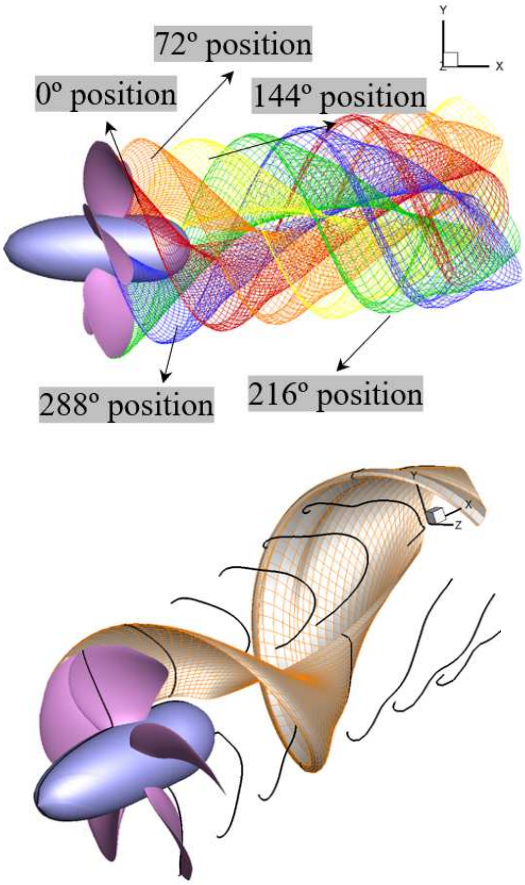


**Figure 1.** The projected view of aligned wake geometries of DTMB4661 propeller with hub which has elliptical ends. Black solid lines in the lower figure represent wake panels corresponding to the intersection of a vertical plane $(x-y)$ through the propeller axis.

Contour plots of vorticity magnitude of points on the $x-y$ and $x-z$ plane, predicted by RANS simulations are overlaid with the wake geometries predicted by BEM in Figure 2 for advance rations of $J_S = 0.8$ and $J_S = 1.0$. As shown, the vorticity gradually diffuses as it is convected downstream. The locations of concentrated vorticity of the trailing wake, predicted by BEM is in good agreement with the locations of the diffused vorticity predicted by RANS simulations. Note the curling of tip vortex predicted by BEM brings more panels around the curling region. It also corresponds to RANS results which show strong vortex magnitude due to tip vortex shed from the blade tip.

The forces predicted by BEM, using the unsteady wake model, are shown in Figure 3, together with the results from RANS at four different advance ratios, i.e., 0.8, 1.0, 1.2, and 1.4. Overall, two methods seem to agree well with each other, especially around the design advance ratio, $J_S = 1.0$. Note the forces (torque coefficients and thrust coefficients) from RANS are evaluated at each time step during the 10 revolutions until it converges, while BEM shows the results only at the last revolution. BEM requires at least three to five wetted revolutions to fully align the wake in an unsteady manner, and consequently, to make the predicted forces converge.

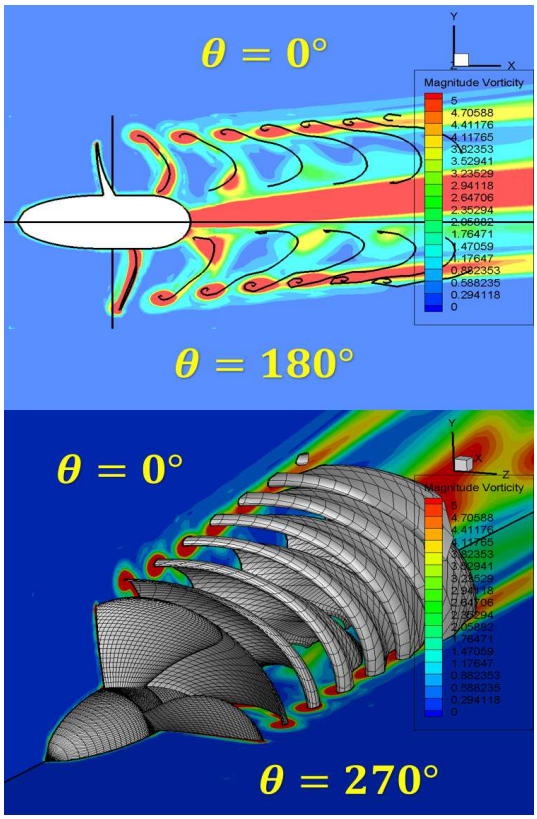


(a)

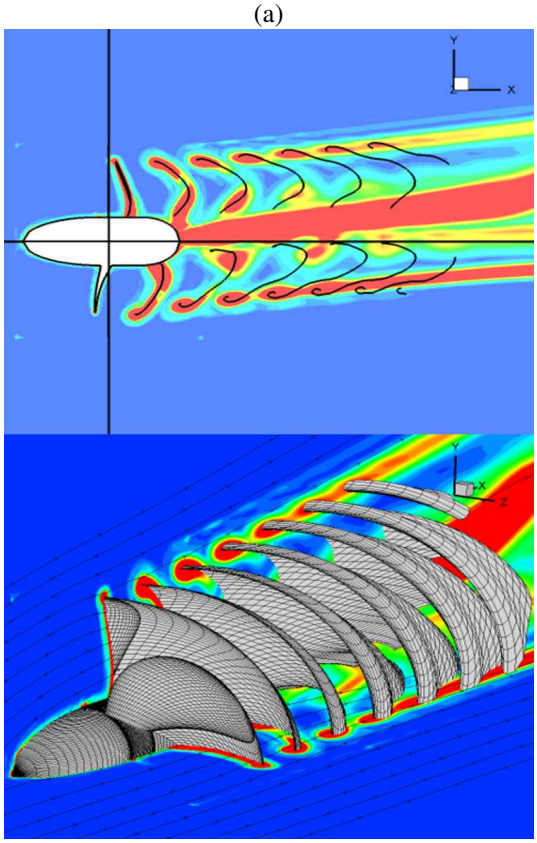

(b)

**Figure 2.** Comparison of the contour plots of vorticity in wake predicted from RANS, and the trailing wake shapes predicted by BEM (shown in black solid line) for advance ratios of (a) 0.8 and (b) 1.0. All shown quantities and wake shapes correspond to the intersection of a vertical and a horizontal planes through the propeller axis.

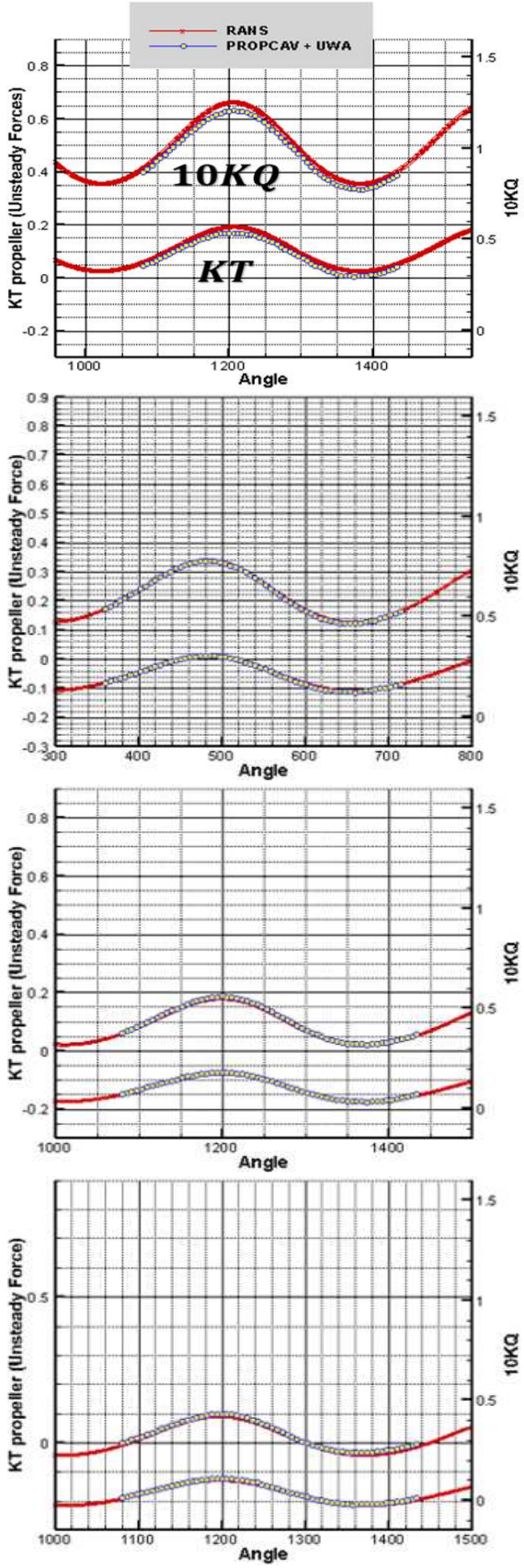


**Figure 3.** Predicted DTMB 4661 propeller performance by BEM using the unsteady wake alignment scheme (denoted by PROPCAV+UWA in the legend), and by RANS in $10^\circ$ inclined shaft flow at advance ratio of $0.8$, $1.0$, $1.2$, and $1.4$ from top to down figure.

### 3.2 Numerical Model (SSPA P2772 Propeller)

Numerical methods are applied to compare their results with the model test data presented in [4], in which a $1:20$ model hull is positioned on the ceiling of the cavitation tunnel, as shown in Figure 4 (up). The geometrical arrangement of the eight transducers used to monitor the pressure signals in the experiment and the fully aligned unsteady wake from BEM are presented in Figure 4 and 6, respectively.

Although the hydrodynamic BEM does not contain the hull geometry when aligning the wake, the effective wake evaluated via BEM/RANS method [16] accounts for the effects of the hull geometry and vortical inflow/propeller interactions. In order to study the effect of the rudder in the predicted propeller-induced hull pressure, a test is made in Su 2018 [16], in which two cases are tested in the pressure-BEM model: one includes only the upper part of the rudder; the other is totally neglecting the rudder geometry as in Figure 7. According to the presented results, the difference is negligible except the transducers relatively close to the reading edge of the rudder. In other words, including the upper part of the rudder affects the predicted hull pressure locally. Based on this, this paper claims that the effect of neglecting rudder geometry is minor and therefore would not affect the results as much.

As shown in Figure 6, the aligned wake from BEM shows lower axial velocity behind the blade tip and near the hub around blade angle $-15^\circ$ to $+15^\circ$. The aligned wake in this region does not advance downstream as much like the wake at other blade angles; therefore, it shows the aligned wake captures the details of inflow variation in the effective wake. It is possible since the unsteady wake alignment scheme considers the non-axisymmetric component of the effective wake such that the wake geometry is a function of radial and tangential directions. Since the results from the BEM are used to calculate the trajectory of the developed tip vortex and the propeller-induced hull pressure, the accurate prediction of the wake geometry is very crucial. For a more elaborate case, such as the case with non-periodic unsteady inflow, it goes beyond the range of this paper and requires BEM/RANS interactive scheme [16].

In the hydrodynamic BEM, $80 \times 20$ panels (chordwise $\times$ spanwise) are used to represent a sing blade geometry. The trailing wake assumes 120 panels in streamwise direction in order to make the tailing wake precede farther to downstream beyond the rear end of the hull. SSPA P27772 propeller is a 4-bladed propeller, which rotates clockwise direction seen from downstream. Constant spacing and full cosine spacing are used to discretize the blade geometry in spanwise and chordwise directions, respectively. Although the hub geometry in the experiments has finite axial length, BEM in this study uses an infinite hub to prevent wake surface from intersecting inside hub radius where the effective wake is unknown or needs to be extrapolated.

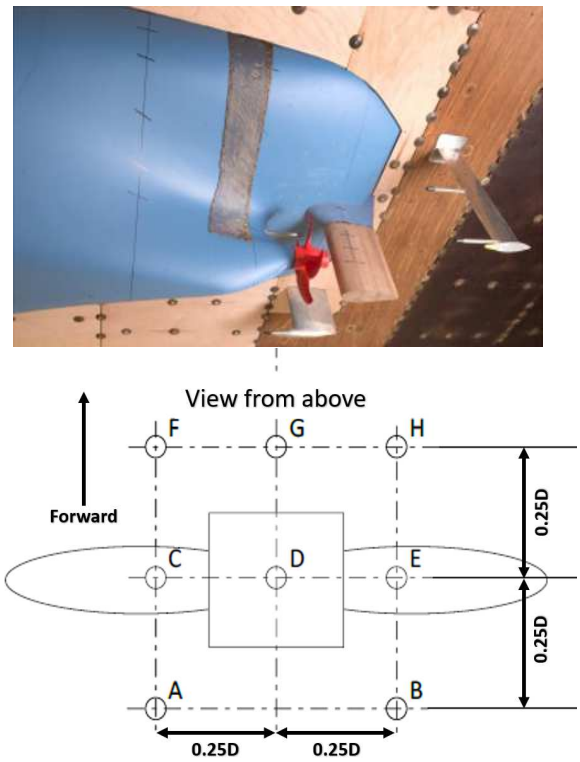


**Figure 4.** Experimental arrangement of SSPA P2772 propeller mounted on the model-scaled ship and the arrangement of pressure transducers, modified from [4]

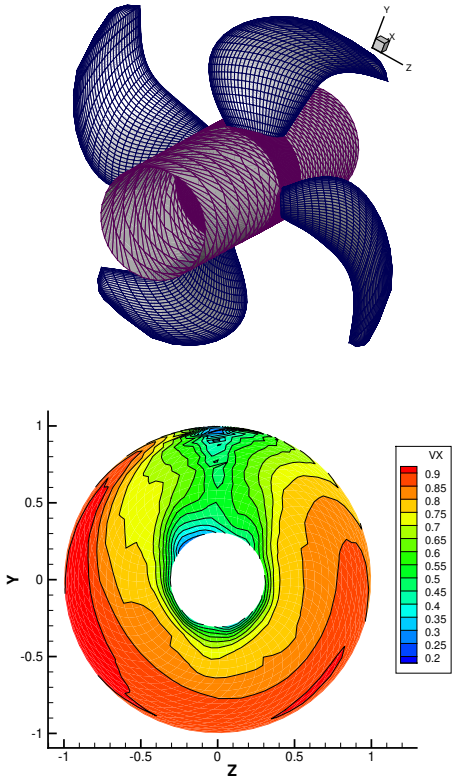


**Figure 5.** Blade geometry (up) and the predicted effective wake field (down) at the advance ratio of $J_S = 0.8082$. The effective wake is evaluated on the mid-chord disk; therefore, the actual effective wake field may vary in the axial direction.

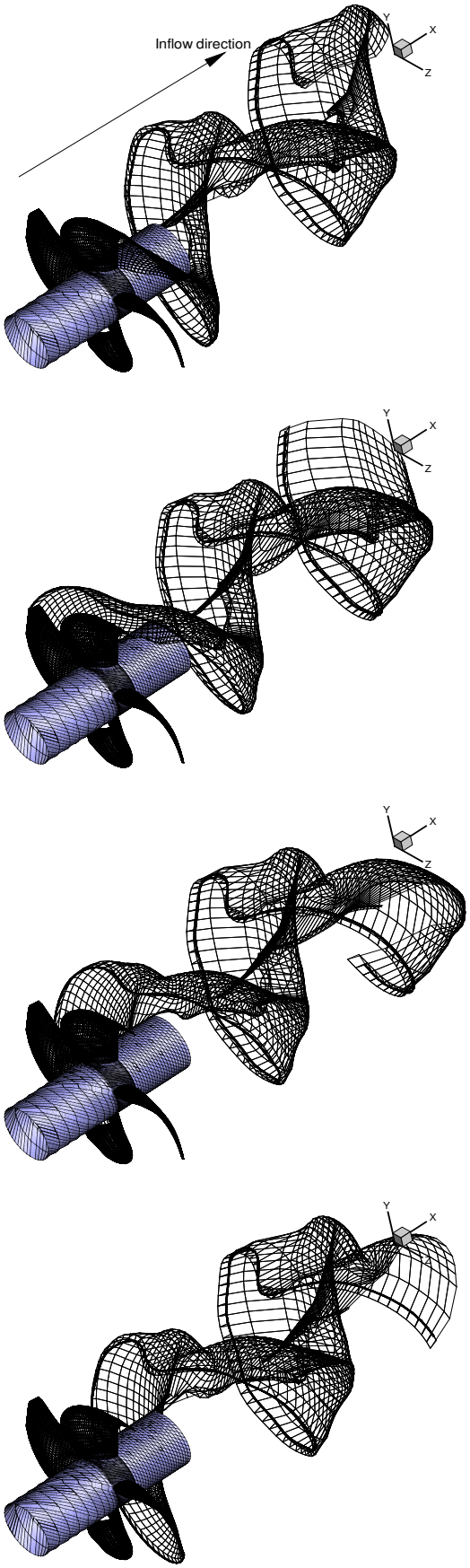


**Figure 6.** Aligned wake geometries for SSPA P2772 propeller with infinite hub at blade angle 0°, 90°, 180°, and 270° up to down figures. Only the key wake is presented.

In the pressure-BEM model, an external flow problem is solved, which means the BEM panels need to be placed on the surface of a closed body. In reality, since the fore part of the hull has very little influence on the propeller-induced pressure, only the aft part of the hull needs to be included in the calculations, as shown in Figure 7. An image hull model is included to consider the free surface effect. In the present methods, as mentioned above, both the wake alignment model and the pressure-BEM model do not consider the rudder geometry. It is because the interaction between the blade trailing wake and the rudder may cause the singular radiated pressures on the rudder surface where the wake panels most likely penetrate the rudder surface.

A cavitating case is also investigated using the hydrodynamic BEM to validate the predicted cavity pattern. SSPA P2772 propeller is operated at $J_S = 0.8082$ and the cavity number $\sigma = 2.9137$ is adopted as reported in the experiments. The predicted cavity patterns from BEM are compared to the photographs taken during the experiments at several blade angles, as shown in Figure 9. Both BEM and the experiments detect a small amount of sheet cavity around $0^\circ$ to $20^\circ$ blade angles, and the comparisons of the cavity patterns are qualitatively in good agreement with each other. The experiment also captures the developed tip vortex as the sheet cavity is replaced by the developed tip vortex cavity beyond $30^\circ$ blade angle. However, the present hydrodynamic BEM assumes the developed tip vortex cavity throughout the whole blade revolution omitting the development step, during which the detached tip vortex is moving closer and eventually attached to the blade tip to become the developed tip vortex. Although this omitting is somewhat violation of physical behavior of the tip vortex, this paper focuses on the effect of tip vortex thickness on the hull pressure by testing different tip vortex radii. Three different radii, i.e., 0.5%, 1.0%, and 2.0% of the blade radius are tested, among which 1.0% case is presented in Figure 8.

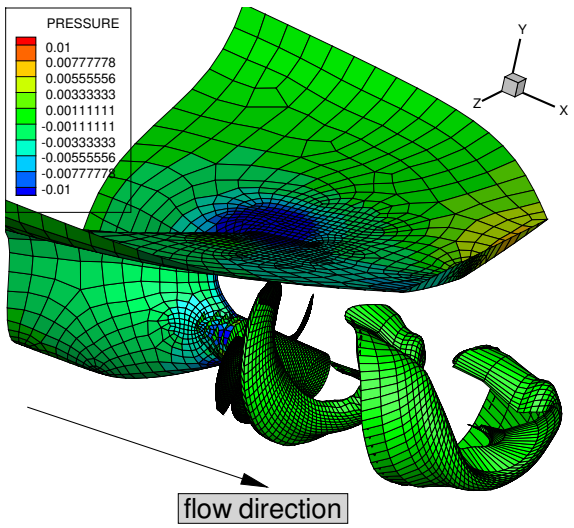


**Figure 7.** Pressure-BEM model without rudder using unsteady wake (only the key wake is presented). Contour plot represents the pressure fluctuation amplitude on the hull. The fore part of the hull is not included in the calculations.

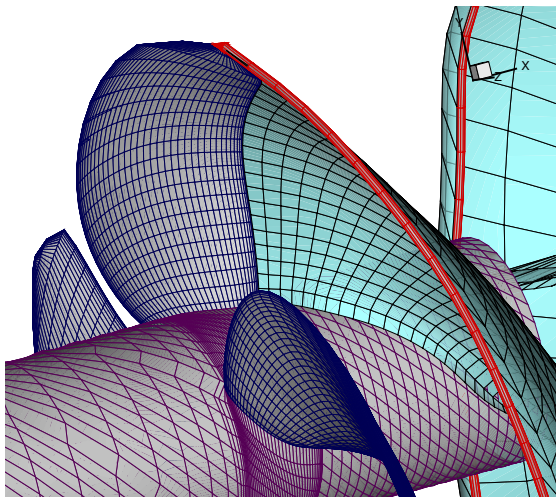

**Figure 8.** The developed tip vortex (in red color) mounted on blade/wake tip with 1.0% vortex core radius.

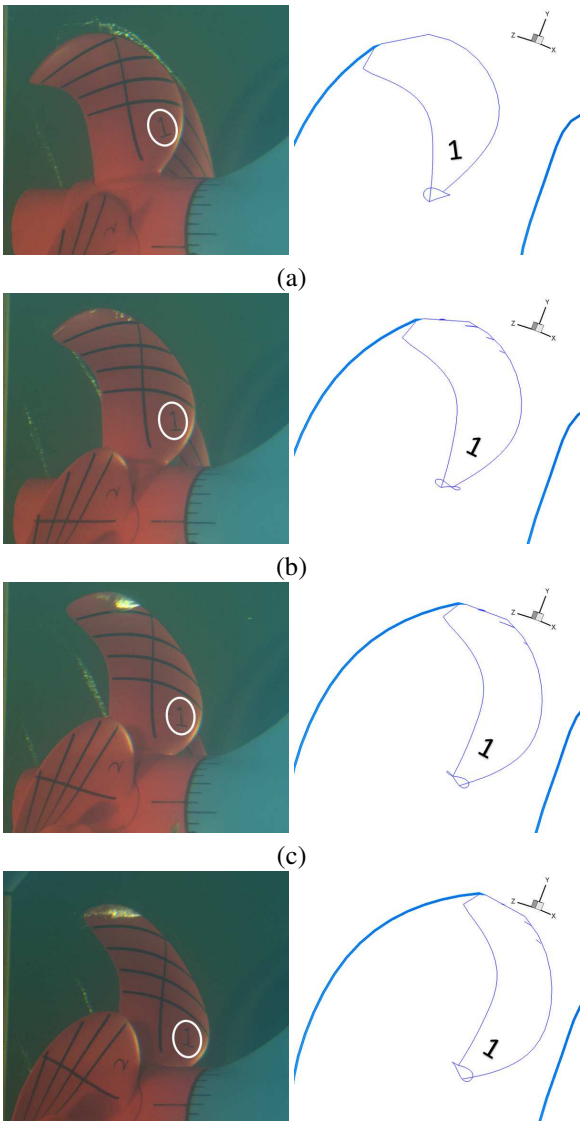


**Figure 9.** The cavity patterns from BEM (right) and the experiment (left) at angular positions (a) $350^\circ$, (b) $0^\circ$, (c) $10^\circ$, and (d) $20^\circ$. The blade on which the cavity is mainly detected is labeled the number 1 to indicate the key blade.

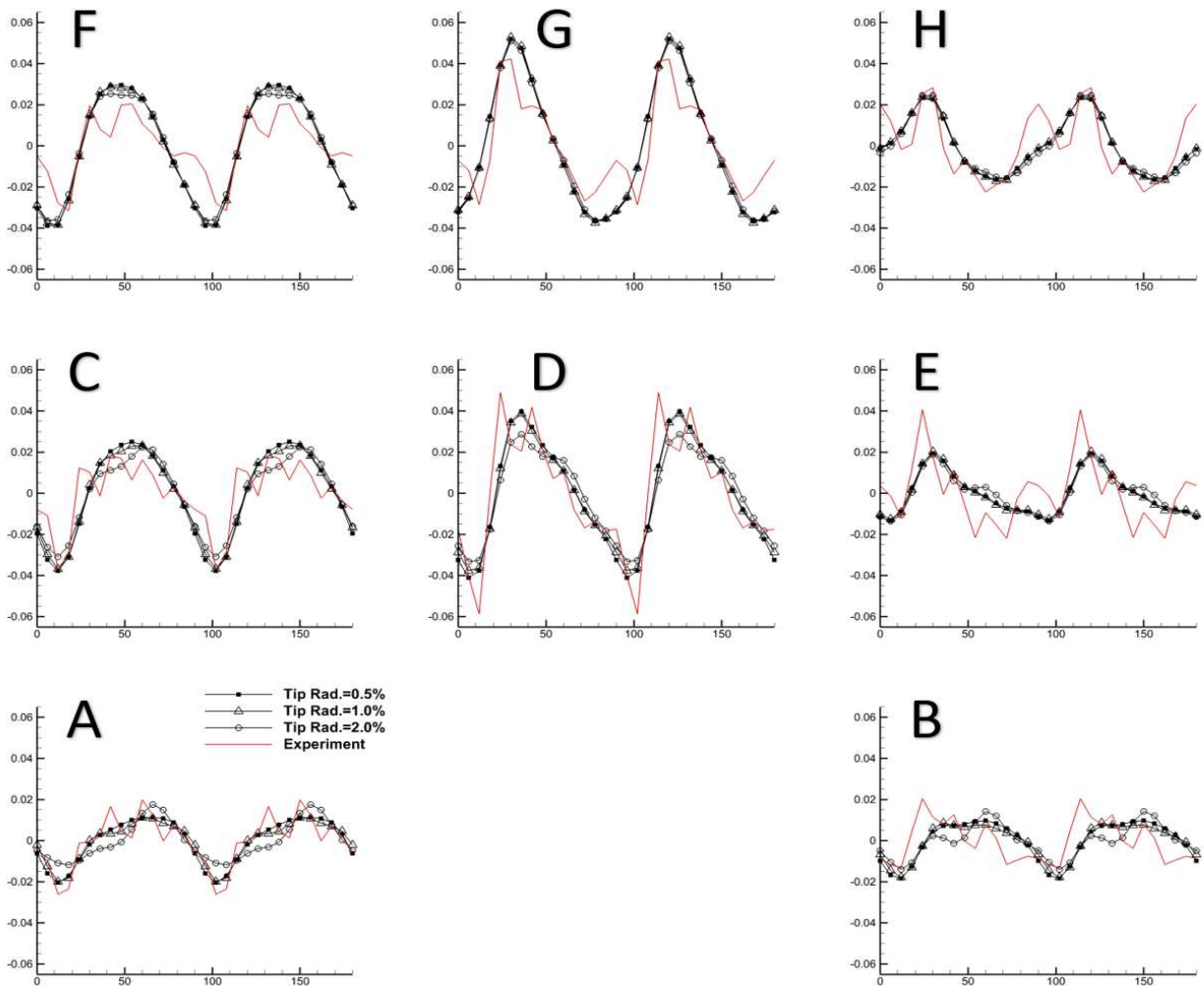


**Figure 10.** Comparison of hull pressures predicted by the pressure-BEM solver with different tip vortex radii. Hull pressure (coefficients) fluctuation with respect to the blade angle from $0^\circ$ to $180^\circ$ due to periodicity. $0.5\%$ tip radius in the legend means the length of the tip vortex radius is as wide as $0.5\%$ of blade radius. Transducer location is indicated in each figure.

The predicted hull pressure fluctuation is also compared to the experimental data, where eight pressure transducers are placed on the hull surface above the propeller. The arrangement of the transducers is shown in Figure 4 (bottom). The pressure histories are recorded under the same load condition as the experiment. Figure 10 compares the pressure history predicted by the acoustic BEM with that from the measurements. As shown, the current method can predict the peak amplitude on most transducer locations. In the cases where the tip vortex radius is small, i.e., $0.5\%$ and $1.0\%$ of the propeller radius, predicted hull pressure does not change with vortex radius significantly. However, as the radius keep increasing beyond $1.0\%$, pressure signal starts to capture a high-frequency component, which the smaller radii cannot detect due to the relatively larger gap between the developed tip vortex and ship hull, as shown on transducers $A$, $B$, $C$, $D$, and $E$. On transducers $F$, $G$, and $H$, different tip vortex radii do not affect the predicted hull pressure as much since these transducers are located upstream of the propeller. For the same reason, other transducers located relatively downstream show noticeable differences in both the peak amplitude and fluctuating frequency as vortex radius increases. This is because the non-axisymmetric component of the effective wake brings more tip vortex and wake panels toward the hull so that they have a stronger influence on the hull pressure. On transducer $E$, the fluctuating pressure from BEM underpredicts the fluctuating pressure amplitude since the effective wake is not symmetric about the ship center; therefore, either the wake alignment scheme or the tip vortex model might underestimate the pressure purses on one side of the hull.

The exact shape of the tip vortex, which satisfies the dynamic boundary condition, is expected to improve the correlations with the experiments since it allows the present method to detect a high-frequency component. The dynamic boundary condition requires the pressure on the cavity surface to be constant and equal to the cavity pressure $P = P_C$ by adjusting vortex radius using the two-point Newton-Raphson method. Details of the determination of

tip vortex cavity shape can be found in Lee 2004 [11]. Now that the inception stage of tip vortex cavity is excluded in this study as mentioned earlier, tip vortex is assumed to be fully developed and attached to the blade tip from the beginning. Besides, the vorticity of tip vortex is assumed to be concentrated inside a vortex core. If the inception phase is fully accounted for, with the changes in tip vortex radii, pressure predictions could be improved by detecting a high-frequency component as shown in the $2.0\%$ radius case. This is another future topic of this research.

## CONCLUSIONS

The propeller-induced hull pressure is predicted for SSPA P2772 propeller in cavitating condition. The unsteady wake alignment scheme is used to make the wake panels fully aligned based on the local unsteady flow. The wake alignment scheme is very crucial in determining the dipole strength on blade, and therefore predicting the cavity patterns under the non-axisymmetric effective wake. A hybrid BEM/RANS method is first used to evaluate the effective wake on the mid chord disk, and the hydrodynamic BEM and acoustic BEM are applied subsequently to solve for the radiated potentials on the hull. The predicted cavity patterns from the hydrodynamic BEM are compared qualitatively well to those from the experiments. Including the developed tip vortex cavity model shows that a high-frequency component on hull pressure signal starts to appear as the tip vortex radius increases. The high frequency component was not evident in the thinner radius case since it has minor influences on the fluctuating hull pressure due to the relatively large distance from hull surface. Overall prediction is expected to be improved by satisfying the dynamic boundary condition on the tip cavity surface, as this will provide changes in the tip vortex cavity both in space and in time. The tip vortex cavity shape in space and time will be determined iteratively by requiring the pressure on cavity surface to be equal to the cavity pressure. Future work includes studying the blade boundary layer effect on the hull pressure, incorporating the unsteady wake-rudder interaction in the numerical scheme, and studying the effect of a finite speed of sound.

## ACKNOWLEDGEMENTS

Support for this research was provided by the US Office of Naval Research (Grant Number N00014-14-1-0303 and N00014-18-1-2276; Dr. Ki-Han Kim) partly by Phase VIII of the "Consortium on Cavitation Performance of High Speed Propulsors".

## REFERENCES

R. Arndt, V. Arakeri, and H. Higuchi. Some observations of tip-vortex cavitation. *Journal of Fluid Mech.*, 229:269–289, 1991.

R. Boswell, S. Jessup, K. Kim, and D. Dahmer. Single-blade loads on propellers in inclined and axial flows. Tecnical Report DTNSRDC-84/084, DTNSRDC, 1984.

J. P. Breslin, R. J. Van Houten, J. E. Kerwin, and C-A. Johnsson. Theoretical and experimental propeller-induced hull pressures arising from intermittent blade cavitation, loading, and thickness. *The Society of Naval Architects and Marine Engineers*, 1982.

J. Hallander and L. Gustafsson. Aquo model test for m/t olympus. Tecnical Report RE40116086-01-00-A, SSPA Sweden AB, Sweden, November 2013.

L. He and S. A. Kinnas. Numerical simulation of unsteady propeller/rudder interaction. *International Journal of Naval Architecture and Ocean Engineering*, 9(6):677–692, November 2017.

Y. Hwang, H. Sun, and S. A. Kinnas. Prediction of hull pressure fluctuations induced by single and twin propellers. *Propellers/Shafting '06 Symposium, SNAME*, 2006.

S. Kim. An improved full wake alignment scheme for the prediction of open/ducted propeller performance in steady and unsteady flow. Master's thesis, Ocean Engineering Group, UT Austin, August 2017.

S. Kim, S. A. Kinnas, and W. Du. Panel method for ducted propellers with sharp trailing edge duct with fully aligned wake on blade and duct. *Journal of Marine Science and Engineering*, 6(89), 2018.

S. Kim, Y. Su, A. Du, and S. A. Kinnas. PROPCAV (version r2018a) user's manual. Ocean Engineering Report 18-2, Ocean Engineering Group, UT Austin, Austin, TX, October 2018.

S. Kim, Y. Su, and S. A. Kinnas. Prediction of the propeller-induced hull pressure fluctuation via a potential-based method: Study of the influence of cavitation and different wake alignment scheme. *CAV2018*, 2018.

H. Lee and S. A. Kinnas. Application of bem in the prediction of unsteady blade sheet and developed tip vortex cavitation on marine propellers. *Journal of Ship Research*, 38(1):15–30, March 2004.

K. Lee, J. Lee, D. Kim, K. Kim, and W. Seong. Propeller sheet cavitation noise source modeling and inversion. *Journal of Sound and Vibration*, 333(5):1356–1368, 2014.

H. Seol, J. Suh, and S. Lee. Development of hybrid method for the prediction of underwater propeller noise. *Journal of Sound and Vibration*, 288(1):345–360, 2005.

Y. Su, S. Kim, W. Du, S. A. Kinnas, M. Grekula, J. Hallander, and Q. Li. Prediction of the propeller-induced hull pressure fluctuation via a potential-based method: Study of the rudder effect and the effect from different wake alignment methods. *Fifth International Symposium on Marine Propulsion (SMP'17), Espoo, Finland*, 2017.

Y. Su, S. Kim, and S. A. Kinnas. Prediction of propeller-induced hull pressure fluctuations via a potential-based method: Study of the effect of different wake alignment methods and of the rudder. *Journal of Marine Science and Engineering*, 6(52), 2018.

Y. Su and S. A. Kinnas. A time-accurate bem/urans in-

teractive method for predicting propeller performance considering unsteady hull/propeller/rudder interaction. *32nd Symposium on Naval Hydrodynamics*, August 2018.

Y. Tian and S. A. Kinnas. A wake model for the prediction of propeller performance at low advance ratio. *International Journal of Rotating Machinery*, 2012(372364), 2002.